The Astronomical Journal, 118:1645–1656, 1999 October

ABUNDANCES OF RED GIANTS IN THE ANDROMEDA II DWARF SPHEROIDAL GALAXY

Patrick Côté[1]
California Institute of Technology, Mail Stop 105-24, Pasadena, CA 91125; pc@astro.caltech.edu
J. B. Oke
California Institute of Technology, Mail Stop 105-24, Pasadena, CA 91125; and Dominion Astrophysical Observatory, Herzberg Institute of Astrophysics, National Research Council of Canada, 5071 West Saanich Road, Victoria, BC V8X 4M6, Canada; bev.oke@hia.nrc.ca
and
Judith G. Cohen
California Institute of Technology, Mail Stop 105-24, Pasadena, CA 91125; jlc@astro.caltech.edu
Received 1999 May 11; accepted 1999 June 17

ABSTRACT

We have obtained spectra for 50 candidate red giants in Andromeda II, a dwarf spheroidal companion of M31, using the Low Resolution Imaging Spectrometer on the Keck II Telescope. After eliminating background galaxies and Galactic foreground stars, we are left with a sample of 42 red giants for which membership in Andromeda II can be established unambiguously from radial velocities. Line indexes measured on the Lick/IDS system are combined with *VI* photometry obtained with the Keck II and Palomar 5 m telescopes to investigate the age and metallicity distribution of these stars. Based on a comparison of the measured line indexes with those of Lick/IDS standard stars in globular and open clusters, we derive a mean metallicity of $\langle[\mathrm{Fe/H}]\rangle = -1.47 \pm 0.19$ dex. This confirms the earlier conclusion, based on Thuan-Gunn *gr* photometry, that Andromeda II obeys the familiar relation between mean stellar metallicity and galaxy luminosity. There is also evidence for a dispersion in metallicity of $\sigma([\mathrm{Fe/H}]) = 0.35 \pm 0.10$ dex, based on the scatter in the measured Mg *b* line indexes and the observed width of the galaxy's giant branch. We note that, while existing observations of Local Group dwarf galaxies indicate that their mean metallicity depends rather sensitively on total luminosity, the internal *spread* in metallicity appears to be relatively independent of galaxy luminosity.

Our spectroscopic sample contains one carbon star. We measure $M_I \simeq -3.8$ for this star, which places it below the tip of the red giant branch and suggests a common origin with the CH stars found in the Galactic halo. Although this carbon star alone does not provide evidence of an intermediate-age component in Andromeda II, two other stars in our spectroscopic sample have $M_I \simeq -4.7$ and -4.5. Membership in Andromeda II is unambiguous in both cases, indicating that these stars fall along an extended asymptotic giant branch and pointing to the presence of a modest intermediate-age population in this galaxy.

Key words: galaxies: abundances — galaxies: evolution — galaxies: individual (Andromeda II) — galaxies: structure — stars: abundances

1. INTRODUCTION

Andromeda II (And II) is a faint dwarf spheroidal (dSph) galaxy located approximately 10° from the center of M31. It was discovered, along with two other dSph companions of M31, by van den Bergh (1972), who visually searched an area of ~ 700 deg^2, using plates taken with the Palomar Schmidt telescope. Recently, three new M31 dSph galaxies have been discovered, bringing the total number of dSph galaxies associated with M31 to six (Armandroff, Davies, & Jacoby 1998; Armandroff, Jacoby, & Davies 1999; Karachentsev & Karachentseva 1999). Although these systems have been studied to differing extents, existing observations suggest that they bear a remarkable similarity to the dSph galaxies that belong to the Milky Way (e.g., Da Costa et al. 1996; Armandroff et al. 1998, 1999; Hopp et al. 1999; Grebel & Guhathakurta 1999; Caldwell 1999).

Several curious properties of the Galactic dSph's motivate the study of dSph's associated with other galaxies. First, their large central velocity dispersions indicate that they contain significant dark matter components (Aaronson 1983; Faber & Lin 1983; Mateo 1998). Second, color-magnitude diagram (CMD) studies reveal detailed and extraordinarily varied star formation histories (Da Costa 1992; Smecker-Hane et al. 1994; Stetson, Hesser, & Smecker-Hane 1998). Last, in many cases, the observed metallicity distribution functions indicate surprisingly wide ranges in metallicity and thus point to complex chemical-enrichment histories (Canterna 1975; Zinn 1978; Shetrone, Bolte, & Stetson 1998).

The presence of intermediate-age stars in these galaxies complicates the derivation of metallicity distribution functions based on broadband photometry alone. For most of the Galactic dSph's, spectroscopic metallicity determinations for individual red giants are now available (e.g., Da Costa et al. 1991; Suntzeff et al. 1993; Ibata et al. 1997). However, existing constraints on the metallicities of the dSph's associated with M31 come entirely from broadband photometry (Armandroff et al. 1993; Da Costa et al. 1996; Hopp 1999; Grebel & Guhathakurta 1999). In the case of And II, the sole metallicity determination comes from Thuan-Gunn *gr* photometry obtained with the 4-Shooter CCD camera on the Palomar 5 m telescope (König et al. 1993, hereafter KNMF). Based on the location and width of the red giant branch (RGB), these authors reported a mean

[1] Sherman M. Fairchild Fellow.

TABLE 1

CANDIDATE RED GIANTS IN ANDROMEDA II OBSERVED WITH LRIS

ID	α (J2000.0)	δ (J2000.0)	V (mag)	$V-I$ (mag)	g (mag)	$g-r$ (mag)	KNMF	Comments
1	01 16 22.11	33 25 59.2	22.26	1.36	21.84	0.72	NE-382	Member
2	01 16 24.19	33 25 51.0	22.42	1.75	21.80	0.94	NE-228	Member
3	01 16 26.52	33 25 41.8	22.33	1.92	22.00	0.92	NE-062	Member (?); carbon star
4	01 16 25.19	33 25 31.9	21.91	1.62	21.48	0.80	NE-161	Member
5	01 16 21.77	33 25 06.2	21.89	1.72	21.64	0.82	SE-227	Member
6	01 16 21.16	33 24 57.6	22.37	1.44	23.00	0.37	SE-267	Member
7	01 16 22.80	33 24 48.7	22.29	1.67	22.02	0.76	SE-185	Member
8	01 16 26.96	33 24 39.4	22.17	1.93	21.69	1.08	SE-041	Member
9	01 16 27.34	33 24 30.6	22.43	2.50	21.93	1.12	SE-034	Nonmember
10	01 16 25.63	33 24 21.3	22.30	1.51	22.27	0.35	SE-084	Member
11[a]	01 16 25.24	33 24 11.5	21.94	1.63	21.74	0.64	SE-098	Member
12	01 16 27.34	33 24 00.1	22.25	2.01	22.00	0.73	SE-035	Member
13	01 16 24.76	33 23 40.7	22.19	1.75	22.02	0.97	SE-053	Member
14	01 16 23.50	33 23 26.7	22.03	2.53	21.06	1.40	SE-153	Member
15	01 16 20.68	33 23 18.1	22.02	1.52	21.59	0.91	SE-289	Member
16	01 16 19.33	33 23 07.2	22.19	1.72	21.76	1.17	SE-319	Member
17	01 16 22.73	33 22 56.2	21.96	1.50	21.63	0.74	SE-188	Member
18	01 16 24.93	33 22 45.8	21.69	1.65	21.39	0.68	SE-104	Member
19	01 16 27.35	33 22 23.0	21.67	1.38	...	...	...	Member
20[a]	01 16 23.56	33 21 49.1	22.20	1.36	22.05	0.43	SE-151	Member
21	01 16 21.87	33 21 37.2	21.89	1.98	...	...	...	Nonmember
22	01 16 21.96	33 21 14.4	21.65	1.69	...	...	...	Member
23	01 16 20.79	33 21 03.0	22.29	1.36	22.70	−0.07	SE-278	Member
24	01 16 24.66	33 20 28.3	21.52	1.31	...	...	...	Nonmember
25	01 16 19.17	33 20 06.6	22.47	1.53	...	...	...	Member
26	01 16 22.27	33 19 50.9	21.82	1.66	...	...	...	Member
27	01 16 24.78	33 19 26.4	22.26	1.38	...	...	...	Low S/N; member
28	01 16 22.10	33 18 59.3	21.77	1.65	...	...	...	Member
29	01 16 22.02	33 26 02.2	22.15	1.49	22.56	0.95	NE-385	Member
30	01 16 26.55	33 25 48.6	21.37	1.65	21.89	0.85	NE-061	Member
31	01 16 19.54	33 25 32.4	22.49	1.11	22.48	0.30	NE-552	Low S/N; membership uncertain
32	01 16 25.31	33 25 10.5	21.82	1.81	...	...	...	Member
33	01 16 23.67	33 24 59.3	22.16	1.72	22.51	0.70	SE-146	Member
34	01 16 19.86	33 24 50.1	22.19	1.48	...	...	...	Member
35	01 16 20.77	33 24 37.1	22.14	1.46	22.57	0.67	SE-276	Member
36	01 16 27.49	33 24 25.8	22.05	1.78	22.45	0.63	SE-032	Member
37	01 16 21.17	33 24 02.5	22.03	1.56	22.45	0.82	SE-259	Member
38	01 16 23.07	33 23 42.0	22.61	1.56	22.68	0.70	SE-172	Emission-line galaxy; $z = 0.55$
39	01 16 23.16	33 23 23.3	22.20	1.88	22.94	1.30	SE-166	Member
40	01 16 26.55	33 23 08.6	22.52	1.76	22.99	0.97	SE-053	Member
41	01 16 19.43	33 22 56.1	22.84	2.70	23.52	1.42	SE-317	Nonmember
42	01 16 24.25	33 22 40.2	22.40	1.41	22.72	0.54	SE-129	Member
43	01 16 19.70	33 21 38.8	22.51	1.47	...	...	...	Member
44	01 16 22.47	33 21 20.3	22.79	1.66	...	...	...	Member
45	01 16 20.15	33 21 09.0	21.82	1.49	...	...	...	Member
46	01 16 26.92	33 20 31.9	22.69	2.18	...	...	...	Low S/N; membership uncertain
47	01 16 23.97	33 20 14.8	22.45	1.36	...	...	...	Member
48	01 16 20.26	33 19 56.6	21.78	1.53	...	...	...	Member
49	01 16 21.92	33 19 31.8	22.04	1.93	...	...	...	Member
50	01 16 22.26	33 19 01.3	22.12	1.50	...	...	...	Member

NOTE.—Units of right ascension are hours, minutes, and seconds, and units of declination are degrees, arcminutes, and arcseconds.
[a] Object included on both LRIS masks.

metallicity of $\langle[\mathrm{Fe/H}]\rangle = -1.59^{+0.44}_{-0.12}$ dex and an internal dispersion of $\sigma([\mathrm{Fe/H}]) \sim 0.43$ dex. However, the possible existence of intermediate-age stars in this galaxy (Aaronson et al. 1985) raises concerns that spreads in both metallicity and age may be contributing to the observed width of the giant branch. Clearly, spectroscopic information and/or ultradeep *Hubble Space Telescope* imaging (such as that presented by Da Costa et al. 1996 for And I) is required to break the well-known "age-metallicity degeneracy" in this and other M31 dSph's. In this paper, we investigate the chemical abundances of individual red giants in And II, using intermediate-resolution ($R \simeq 6$ Å) spectra obtained with the Keck II Telescope; this is the first such study for any dSph galaxy beyond the Milky Way.

2. OBSERVATIONS AND REDUCTIONS

2.1. *Photometry and Astrometry*

Candidate red giants in And II were selected from a single 600 s V image of And II obtained on 1996 August 17, using

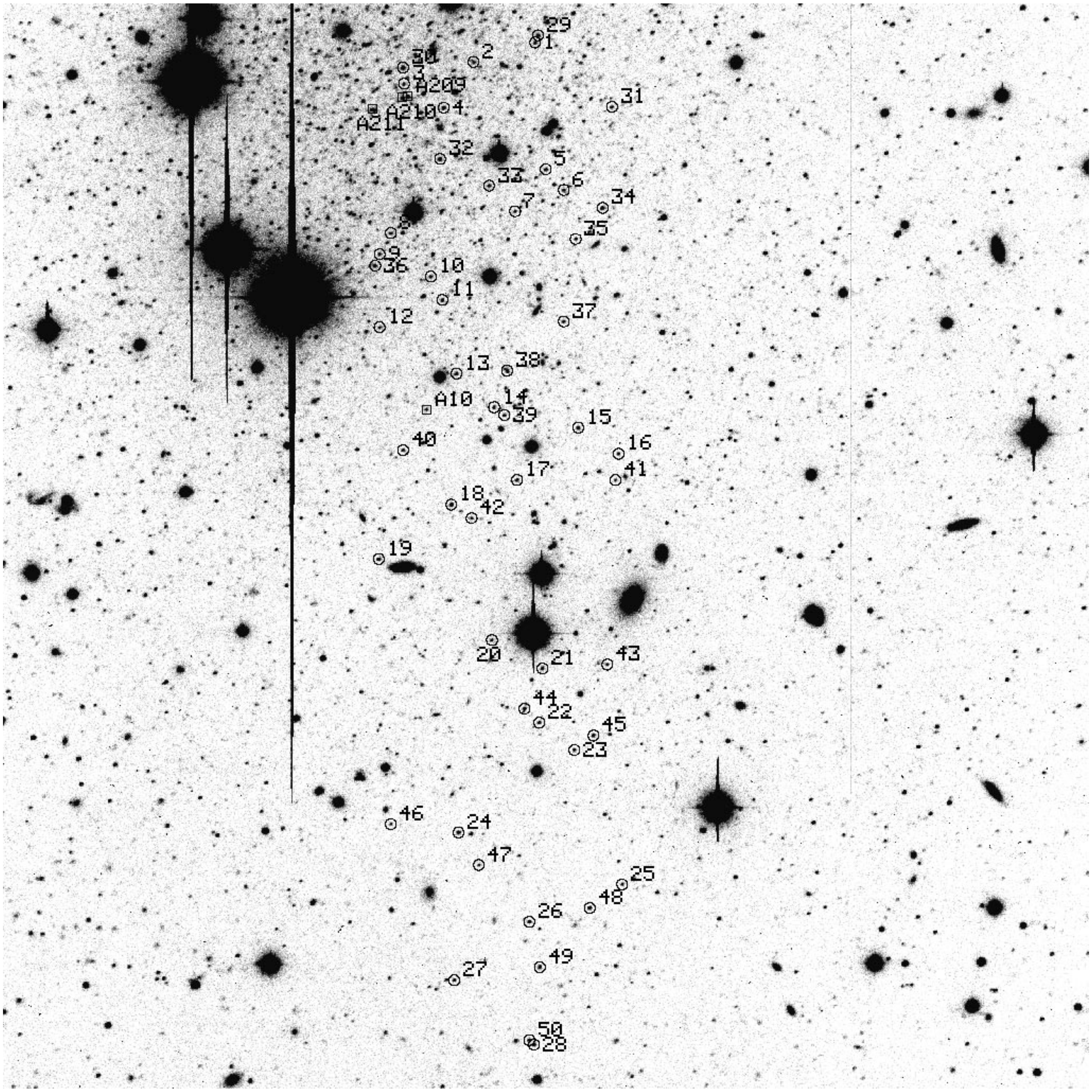

FIG. 1.—Finding chart for And II red giant candidates (*circles*) observed with LRIS in multislit mode. The numbering scheme corresponds to that given in Table 1. North is to the top and east is to the left on this *V*-band COSMIC image, which measures 7′.6 × 7′.6. The four stars observed by Aaronson et al. (1985) are indicated by squares.

the Carnegie Observatories Spectroscopic Multislit and Imaging Camera (COSMIC; Kells et al. 1998) on the Palomar 5 m telescope. COSMIC was used in direct imaging mode, giving a total field of view of 9′.7 × 9′.7. The FWHM of isolated stellar objects in this image was measured to be ∼1″.2. The stand-alone version of DAOPHOT II (Stetson 1987, 1993) was used to measure instrumental magnitudes for 2089 unresolved objects in this field, and stellar objects within the upper ≃1 mag of the RGB were randomly selected for spectroscopic observation with the Keck II Telescope. In a few cases, somewhat brighter objects were added to fill the Low Resolution Imaging Spectrometer (LRIS) slit mask. Absolute positions for these candidate red giants were calculated using the positions of 32 bright stars taken from the USNO-A2.0 catalog (Monet et al. 1996).

On 1996 October 7, *V* and *I* images of And II were taken with LRIS (Oke et al. 1995) on the Keck II Telescope. Exposure times were 600 s in *V* and 300 s in *I*. The FWHM of unresolved objects in these images was measured to be 0″.88 and 0″.76, respectively. The images were bias-subtracted, trimmed, and flat-fielded using median sky flats obtained during twilight. Profile-fitting photometry was performed using the stand-alone version of DAOPHOT II. Unfortunately, no photometric standard stars were observed on this night, so it was not possible to calibrate the LRIS photometry directly. Instead, the Keck photometry was calibrated by reobserving And II and four

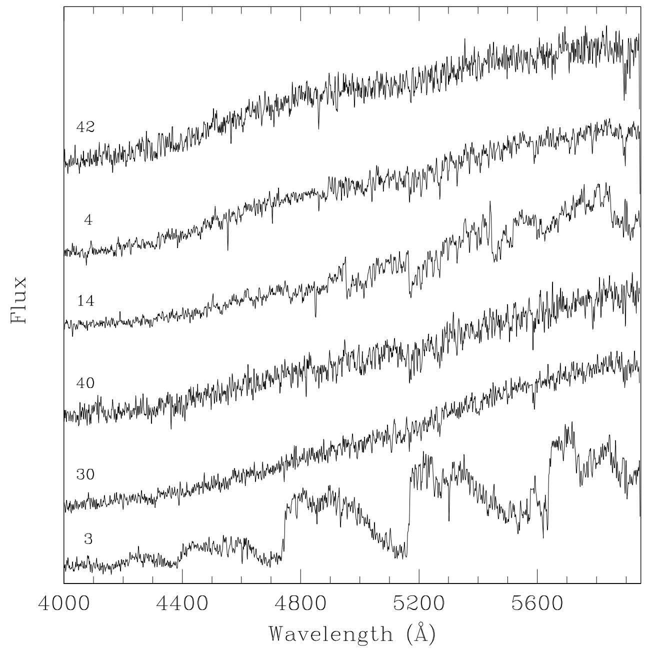

FIG. 2.—Representative sample of LRIS spectra for And II giants. The spectra shown here correspond to program stars that span a wide range in magnitude and color (see Table 1). At 5000 Å, the spectra have 30 $\lesssim$ S/N $\lesssim$ 50 per resolution element. Note the obvious Swan C_2 bands in the spectrum of star 3.

Landolt (1992) standard fields, using the Palomar 5 m telescope and COSMIC on the night of 1998 July 24. Since COSMIC is not equipped with a Cousins *I* filter, a Thuan-Gunn *i* filter was used as a substitute. Based on the residuals between our calculated and observed *V* magnitudes and $V-I$ colors of the Landolt standards, we find standard deviations of 0.04 mag (*V*) and 0.07 mag ($V-I$).

2.2. *Spectroscopy*

Two LRIS masks were designed containing a total of 52 slits: 28 on the first mask and 24 on the second, with two stars (Nos. 11 and 20) included on both masks. On 1996 October 7, we obtained a pair of 3600 s exposures for both masks using a 600 line mm^{-1} grating blazed at 5000 Å. This configuration produced a dispersion of 1.28 Å pixel^{-1} and, when combined with our slit width of 1\".0, a resolution of approximately 6 Å over the range 3950 to 6000 Å. The seeing during the observations was measured to be FWHM $\sim$ 0\".8. Following each exposure, we obtained a comparison spectrum of Hg, Kr, and Ar lamps, which was subsequently used to derive the dispersion solution of the program spectra. Crude radial velocities were measured by cross-correlating the spectrum of each program object against those of red giants in the globular clusters M13, M92, and M71. The radial velocities have a typical uncertainty of $\sigma_{v_r} \sim 40$ km s^{-1}, which, given the heliocentric radial velocity of $\overline{v}_r = -188 \pm 3$ km s^{-1} for And II (Côté et al. 1999), is sufficient for establishing membership. For objects 3, 31, and 46, no radial velocity could be measured; these stars are omitted from the determination of the metallicity of And II.

Table 1 gives the identification number of each candidate red giant observed spectroscopically with LRIS, its right ascension and declination, *V* magnitude, and $V-I$ color. For those objects that are located in both our LRIS field and the 4-Shooter field of KNMF, Table 1 includes the *g* magnitude, $g-r$ color, and star identification number from KNMF. The final column of Table 1 indicates whether the object is a member of And II based on its measured radial velocity (see below). A finding chart for all objects listed in this Table 1 is presented in Figure 1.

Figure 2 shows extracted, wavelength-calibrated, and co-added spectra for six of the And II member giants. The strong C_2 bands in the spectrum of star 3 immediately identify it as a carbon star. Aaronson et al. (1985) reported the presence of carbon stars in And II and suggested on this basis that And II contains a modest fraction of intermediate-age stars. We return to the issue of intermediate-age stars in § 3.2.

3. RESULTS

3.1. *Adopted Distance and Reddening*

The primary goal of this study is the determination of spectroscopic metallicities for individual And II red giants. To do so, we utilize color and reddening information to determine the temperature differences between the program stars and the Lick/IDS standard stars whose line indexes define the metallicity scale (see § 4). Figure 3 shows the (I, $V-I$) CMD for all unresolved objects within 1′ of the galaxy's center. The core radius of And II is $r_c = 1'.89^{+0.47}_{-0.37}$ (Caldwell et al. 1992; Côté et al. 1999), so this selection ensures that the vast majority of the objects plotted in Figure 3 are bona fide And II members. Also shown are globular cluster fiducial giant branches from Da Costa & Armandroff (1990). In the left panel of Figure 3, these have been shifted by $(m-M)_I = 24.22$ and $E(V-I) = 0.08$. These values are appropriate for a Galactic foreground reddening of $E(B-V) = 0.062$ (Schlegel, Finkbeiner, & Davis 1998), $E(V-I) = 1.36\ E(B-V)$ (Taylor 1986; Fahlman et al. 1989), $A_I = 1.86E(B-V)$, and a true distance modulus of $(m-M)_0 = 24.1$. In the right panel, we show the results of adopting $(m-M)_0 = 23.9$, $A_I = 0.15$, and $E(B-V) = 0.08$ (the reddening assumed by KNMF). In what follows, we adopt the reddening deduced from the DIRBE maps of Schlegel et al. (1998) and $(m-M)_0 = 24.1 \pm 0.3$, where the rather large uncertainty reflects both the uncertainty in the true reddening toward And II and potential systematic errors in our photometric calibration.

The corresponding distance of $D_{\rm And\,II} = 660 \pm 90$ kpc places And II $\sim 85 \pm 90$ kpc in front of M31, for an adopted distance of $D_{\rm M31} = 745$ kpc (see § 1 of Holland 1998). Based the apparent magnitude of the tip of the RGB in And II, KNMF concluded that it is located $\sim$120 kpc closer than M31, for an assumed M31 distance of $D_{\rm M31} = 700$ kpc. We consider this agreement acceptable given the uncertainties involved in transforming our Thuan-Gunn *i* photometry to the Cousins system.

3.2. *Intermediate-Age Stars?*

Aaronson et al. (1985) presented low signal-to-noise ratio (S/N) spectra for four luminous giants in And II obtained with the Palomar 5 m telescope. Their sample includes one unambiguous carbon star (A211), one possible carbon star (A10), and one M giant (A209). Based on *JHK* photometry for these stars and an *assumed* distance modulus of $(m-M)_0 = 24.3$ for And II, Aaronson et al. (1985) derived bolometric magnitudes of $-4.45 \lesssim M_{\rm bol} \lesssim -4.1$ for these

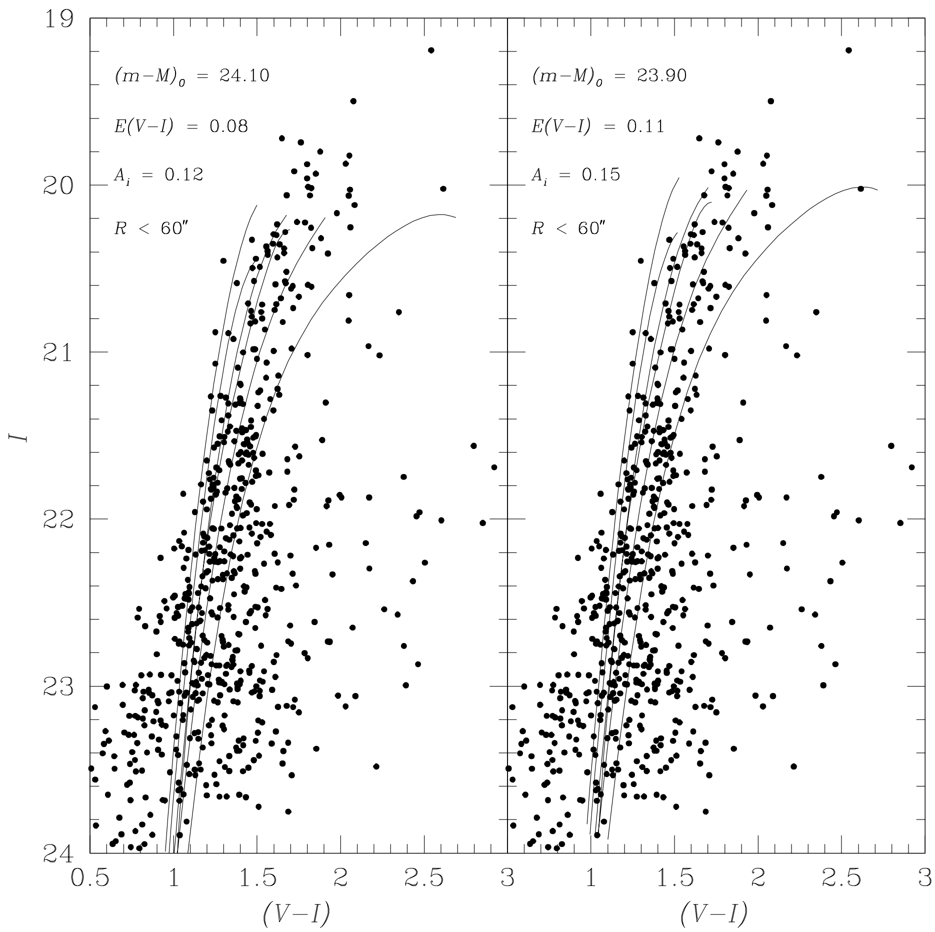

FIG. 3.—(I, $V-I$) CMD for And II. In both panels, only unresolved objects within 60″ of the center of the galaxy are shown, along with fiducial sequences for the red giant branches of six Galactic globular clusters: from left to right, the solid lines are M15 ([Fe/H] = −2.22), NGC 6397 (−1.95), M2 (−1.62), NGC 6752 (−1.55), NGC 1851 (−1.26), and 47 Tuc (−0.76). The left panel shows the fiducial sequences shifted by $E(V-I) = 0.08$, $A_V = 0.12$, and $(m-M)_0 = 24.10$. This reddening corresponds to the value of $E(B-V) = 0.06 \pm 0.01$, indicated by the reddening maps of Schlegel et al. (1998). The right panel shows the same sequences shifted by $E(V-I) = 0.11$, $A_V = 0.15$, and $(m-M)_0 = 23.90$, equivalent to adopting $E(B-V) = 0.08$.

stars and concluded that And II contains at least some intermediate-age stars.

Since CH carbon stars are found in the Galactic halo, as well as in at least two globular clusters (ω Cen and M14; see Harding 1962; Dickens 1972; Côté et al. 1997), the mere existence of carbon stars in And II does not provide unambiguous evidence of an intermediate-age population (although the *absence* of such a population in And II might perhaps be surprising given the emerging evidence for intermediate-age populations in the vast majority of Local Group dSph's; see Mateo 1998; Grebel 1999). On the other hand, carbon stars with $M_I \lesssim -4.0$ (Da Costa & Armandroff 1990) have luminosities that exceed those of the brightest red giants found in metal-poor globular clusters, so it is safe to assume that they are, in fact, intermediate-age objects that have undergone carbon dredge-up during the ascent of the asymptotic giant branch (AGB) and not the end products of mass transfer evolution among compact binaries (McClure 1997).

None of the four stars observed by Aaronson et al. (1985) were included in our spectroscopic sample, although we include these objects in the finding chart given in Figure 1. Curiously, the two certain carbon stars in And II (i.e., our No. 3 and Aaronson No. 211) are separated by only 13″. The location of the four stars studied by Aaronson et al. (1985) in the CMD is shown by the filled squares in Figure 4. We find $-5.0 \lesssim M_I \lesssim -4.2$ for these four stars, confirming the principal conclusion of Aaronson et al. (1985) that these objects belong to an extended AGB population. On the other hand, the newly discovered carbon star has $M_I \simeq -3.8$ and consequently does *not* lie above tip of the RGB. We note that two other member stars (objects 14 and 30, which have $M_I \simeq -4.7$ and -4.5, respectively) are also located above the RGB tip in Figure 4 and are probably, like the four stars identified by Aaronson et al. (1985), members of an intermediate-age component in And II.

4. MEAN METALLICITY AND ABUNDANCE SPREAD

4.1. *The Color-Magnitude Diagram*

Based on the CMDs of And II presented in Figures 3 and 4, we estimate a mean metallicity of $\langle[\mathrm{Fe/H}]\rangle \sim -1.35 \pm 0.3$ dex. This is marginally higher than the value of $\langle[\mathrm{Fe/H}]\rangle \sim -1.59 \pm^{+0.44}_{-0.12}$ dex reported by KNMF, although still consistent within the rather large uncertainties. In addition, we find the width of the RGB to be significantly larger than that expected purely on the basis of the photometric errors. The left panel of Figure 5 shows the (I, $V-I$) CMD for 134 unresolved objects having $21 \le I \le 22$ and lying within 1′ of the galaxy's center. The dotted lines show the fiducial globular cluster red giant branches shown in Figures 3 and 4; the solid line indicates

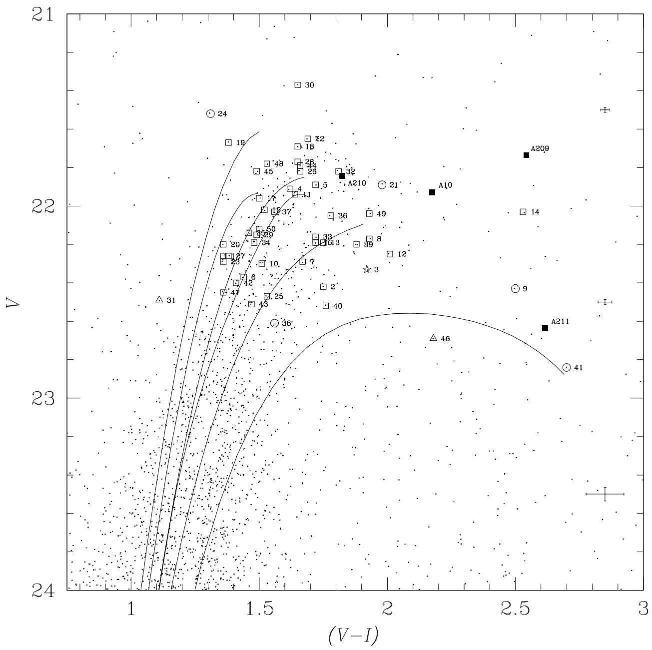

FIG. 4.—(V, $V-I$) CMD for And II. The globular cluster fiducial sequences are the same as in Fig. 2. We have adopted $E(V-I) = 0.08$, $A_V = 0.19$, and $(m - M)_0 = 24.10$. Open squares indicate member giants for which we have LRIS spectra, nonmembers are shown as circles, and triangles indicate objects whose membership in And II is uncertain. A carbon star is indicated by the five-pointed star. The four stars studied by Aaronson et al. (1985) are indicated by the filled squares. Typical internal photometric errors are shown at the right.

our adopted ridgeline for And II. The right panel of Figure 5 shows the histogram of $V-I$ color residuals about this ridgeline. The best-fit Gaussian, which has a dispersion of $\sigma(V-I) = 0.11 \pm 0.03$ mag, has been overlaid for comparison. Since the mean internal photometric uncertainty for objects within this magnitude range is $\sigma(V-I) = 0.05$ mag, we conclude that the intrinsic dispersion in color is roughly $\sigma(V-I) \simeq 0.10$ mag. At the median magnitude of $I = 21.62$ mag for these stars, the gradient in $(V-I)$ color as a function of metallicity is approximately 0.21 ± 0.04 mag dex^{-1}. Thus, if the broadening of the RGB is ascribed entirely to an internal spread in metallicity, inferred dispersion is $\sigma([\mathrm{Fe/H}]) \sim 0.46 \pm 0.17$ dex. Note that this estimate is unlikely to be contaminated by the presence of old, metal-rich AGB stars, since for metallicities similar to that of And II such stars appear in significant numbers for $M_I \gtrsim -1.5$ (see Fig. 5 of Ferraro et al. 1997) whereas our adopted limits correspond to absolute magnitudes of $-3.2 \lesssim M_I \lesssim -2.2$. Nevertheless, the presence of at least some intermediate-age stars in And II suggests that is probably wise to interpret the above estimate an as upper limit on the true metallicity dispersion (cf. Smecker-Hane et al. 1994, who demonstrate that, at least in the case of the Carina dSph, the RGB is relatively narrow despite Carina's multiple star formation episodes).

4.2. *Line Index Measurements*

During Keck/LRIS observing runs in 1996 April, 1996 October, and 1999 April, we collected high-S/N, long-slit

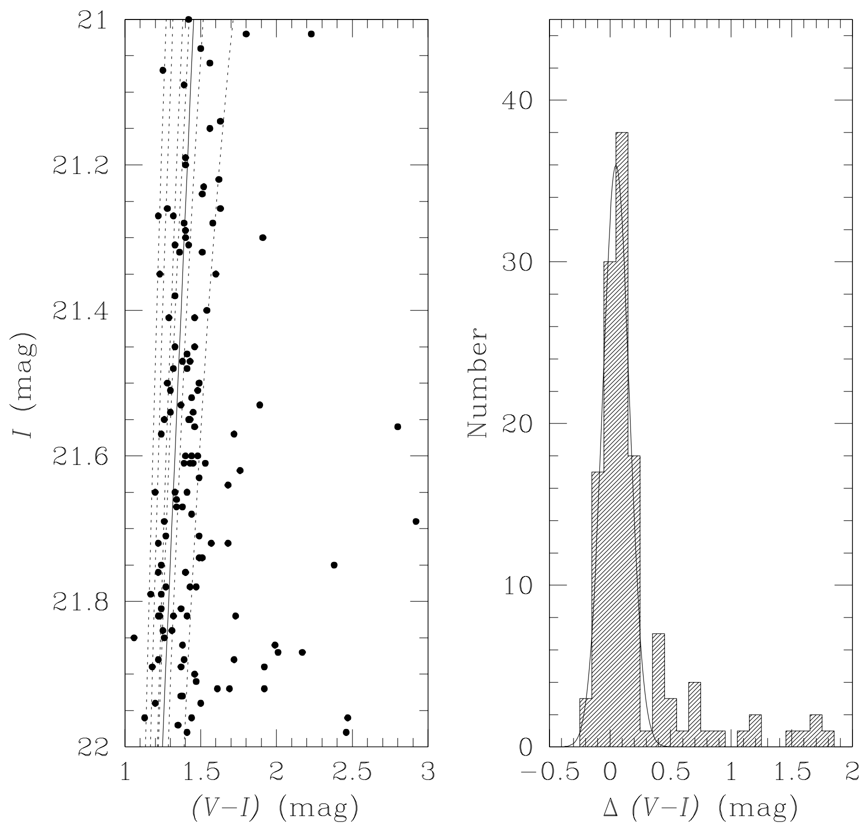

FIG. 5.—*Left*: (I, $V-I$) CMD for all unresolved objects located within 1′ of the center of And II and having $21 \leq I \leq 22$. The dotted lines show the globular cluster fiducial sequences also shown in Fig. 3. The solid line shows the adopted ridgeline for And II; residuals about this line are presented in the right panel. *Right*: Histogram of $V-I$ color residuals for the sample of unresolved objects shown in the left panel. The solid curve is a Gaussian having a dispersion of $\sigma(V-I) = 0.11$ mag. The mean internal photometric uncertainty for the stars in this interval is $\sigma(V-I) = 0.05$ mag. If the intrinsic dispersion in color is ascribed entirely to variations in metallicity, then $\sigma([\mathrm{Fe/H}]) \simeq 0.46 \pm 0.17$ dex (see text for details).

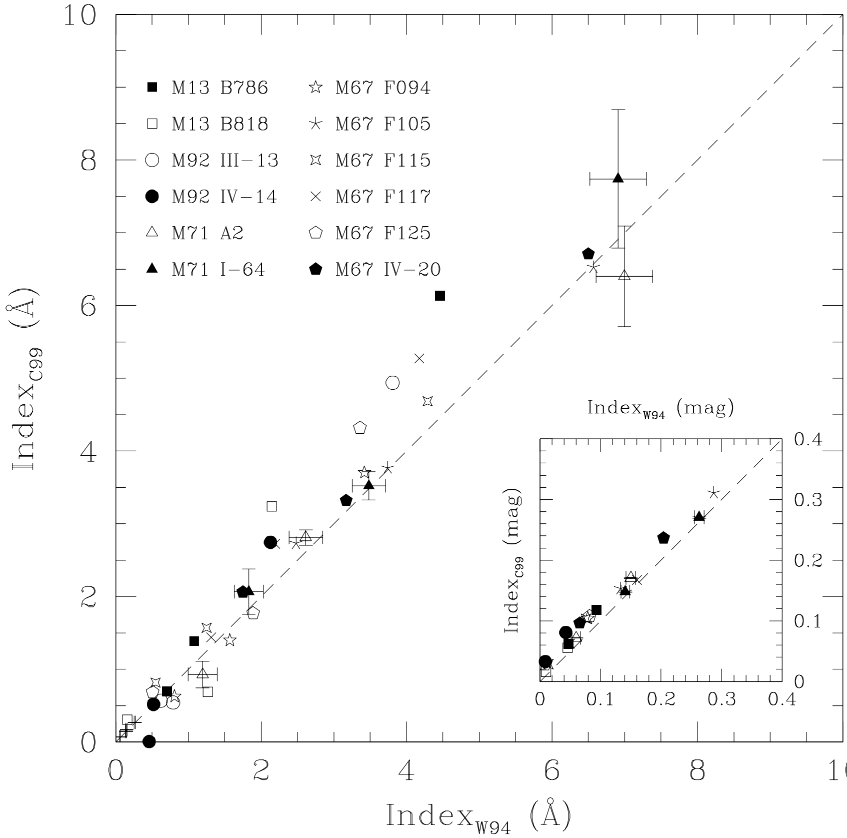

FIG. 6.—Comparison of the G4300, Mg *b*, and Fe5406 line indexes measured from our LRIS spectra ("C99") with those tabulated by Worthey et al. (1994; "W94") for 12 Lick/IDS standards in the clusters M13, M71, M92, and M67. The dashed line shows the one-to-one relation. For clarity, error bars are shown for the two giants in M71 only. *Inset*: Mg $_1$ and Mg $_2$ indexes measured from our LRIS spectra compared with the published values from Worthey et al. (1994). The dashed line shows the one-to-one relation.

spectra for 12 Lick/IDS standard stars in M13, M92, M71, and M67. For M13, long-slit spectra were also measured for eight additional red giants having published $(V-K)_0$ colors (Cohen, Persson, & Frogel 1978). In all cases, the identical grating and central wavelengths were used as for the And II observations, although slits of differing widths were employed for the three runs, i.e., 0″.7, 1″.5, and 1″.0 for the 1996 October, 1996 April, and 1999 October observations, respectively. These slits correspond to spectral resolutions in the range 4 Å $\lesssim$ R $\lesssim$ 9 Å, which are roughly comparable to the resolution of $R = 8$ Å used to define the Lick/IDS indexes (Worthey et al. 1994). All 18 stars are listed in Table 2, which gives the identification number of each star, its absolute magnitude, and $(V-K)_0$ and $(V-I)_0$ colors. These quantities have been taken directly from Cohen et al. (1978), Gorgas et al. (1993), and Worthey et al. (1994), with the exception of $(V-I)_0$, which has been estimated for each star using equation (10) of von Braun et al. (1998). The mean metallicity of the host cluster, taken from the catalog of Harris (1996), is indicated in the final column. Using the index definitions given in Worthey et al. (1994), we have measured absorption-line indexes for each of the stars listed in Table 2. Figure 6 shows our measured line indexes for the 12 Lick/IDS standards plotted against the values given in Worthey et al. (1994). The Na D index was also measured using our program spectra, although it is not considered here since its use is complicated by the existence of interstellar sodium, whose column density is also known to vary significantly over small scales (Cohen 1979; Gebhardt et al. 1994). The two data sets are in good agreement, with the possible exception of a 0.015 mag offset for the Mg $_1$ and Mg $_2$ indexes (in the sense that the Keck spectra yield slightly higher values). The sample of objects is small, however, and we conclude from Figure 6 that our measured indexes are in satisfactory agreement with the published values.

Table 3 lists measured line indexes of 41 red giants belonging to And II. For the Mg $_1$, Mg $_2$, Mg *b*, and Fe5406 indexes, we have imposed a minimum S/N in the local continuum of 15 pixel^{-1}; for G4300, which is the bluest index, this threshold was relaxed to S/N = 10 pixel^{-1}. The uncertainties in the measured indexes have been estimated by adding, in quadrature, the uncertainty due to Poisson noise and with that due to slit alignment errors. The latter is the dominant uncertainty for our measured line indexes since the photon noise in our LRIS spectra never exceeds $\sim$10% pixel^{-1} at 5000 Å. We estimate the uncertainty due to slit alignment errors by shifting each spectrum by $\pm\delta$, where δ is half the width of the slit in wavelength units (e.g., $\delta \sim 3.0$ Å) and remeasuring the value of each line index; the uncertainty is then taken to be half the range spanned by the measurements.

In general, the measured index for any star will be a function of not just metallicity, but also effective temperature and surface gravity. Figure 7 shows the variation in surface gravity as a function of absolute magnitude expected for old, metal-poor, red giants based on the models of Bergbusch & VandenBerg (1992). All of the stars for which we have measured line indexes lie within the

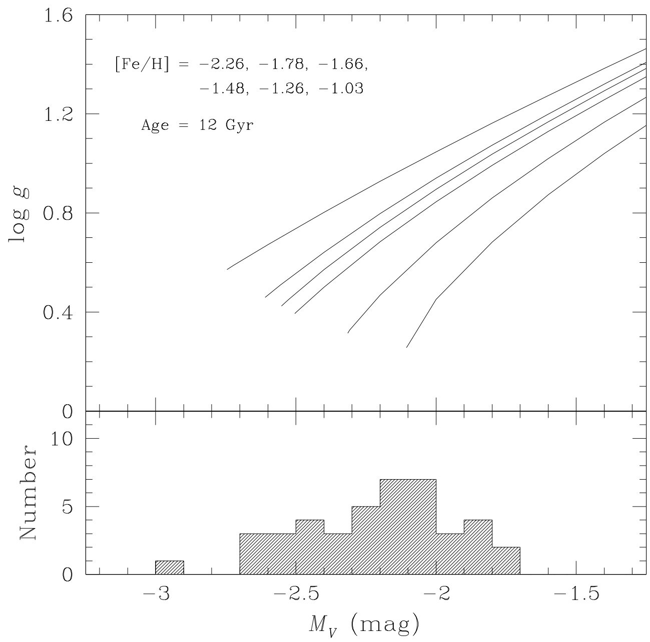

FIG. 7.—*Top*: Surface gravity plotted as a function of absolute visual magnitude for metal-poor red giants of age 12 Gyr (Bergbusch & VandenBerg 1992). From top to bottom, the curves indicate models having [Fe/H] = −2.26, −1.78, −1.66, −1.48, −1.26, and −1.03. *Bottom*: Histogram of absolute visual magnitudes for And II members having measured line indexes. Based on these models, the program stars are expected to have surface gravities in the range $0.4 \lesssim \log g \lesssim 1.2$, with a mean value of $\log g \sim 0.8$.

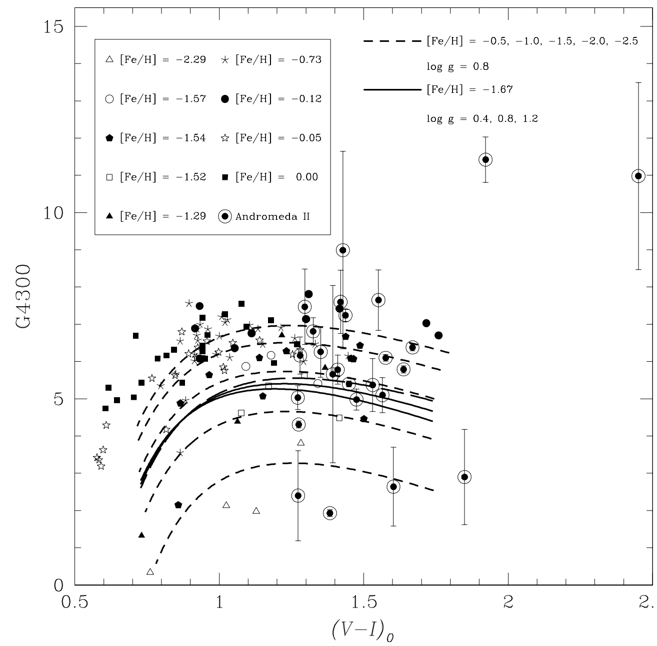

FIG. 8.—G4300 line indexes plotted against $(V-I)_0$ (see text) for Lick/IDS standard stars and And II red giants. The solid and dashed lines show the calibration of Gorgas et al. (1993) for various metallicities and surface gravities. Here [Fe/H] decreases from top to bottom for the dashed lines, and $\log g$ decreases from top to bottom at the red extrema for the solid lines. The indexes for the standard stars are from Gorgas et al. (1993) and Worthey et al. (1994). The symbols correspond to individual stars in the following clusters: M92 ([Fe/H] = −2.29), M3 (−1.57), M13, (−1.54), M10 (−1.52), M5 (−1.29), M71 (−0.73), NGC 7789 (−0.12), M67 (−0.05), and NGC 188 (0.00).

TABLE 2

LICK/IDS STANDARD STARS OBSERVED WITH LRIS

Star	M_V (mag)	$(V-K)_0$ (mag)	$(V-I)_0$ (mag)	[Fe/H] (dex)
Cluster M13:				
B786	−2.23	3.57	1.50	−1.54
B818	−0.29	1.98	0.86	−1.54
I-2[a]	−0.06	2.27	0.97	−1.54
I-24[a]	−1.46	2.72	1.14	−1.54
I-48[a]	−2.27	3.47	1.46	−1.54
II-67[a]	−2.20	3.54	1.49	−1.54
II-76[a]	−1.80	2.95	1.23	−1.54
II-90[a]	−2.09	3.49	1.47	−1.54
III-72[a]	0.81	2.00	0.87	−1.54
IV-25[a]	−2.23	3.43	1.44	−1.54
Cluster M92:				
III-13	−2.57	3.03	1.28	−2.29
IV-114	−0.77	2.35	1.03	−2.29
Cluster M71:				
I-64	−0.30	2.88	1.21	−0.73
A2	1.13	2.19	0.93	−0.73
Cluster M67:				
F094	3.33	1.21	0.58	−0.05
F105	0.80	2.66	1.14	−0.05
F115	3.15	1.30	0.61	−0.05
F117	3.11	1.86	0.82	−0.05
F125	4.36	1.23	0.58	−0.05
IV-20	1.71	2.44	1.05	−0.05

[a] Star not included in Gorgas et al. 1993 or Worthey et al. 1994. $(V-K)_0$ photometry taken from Cohen et al. 1978.

upper ∼1 mag of the And II giant branch, suggesting that these stars have surface gravities in the range $0.4 \lesssim \log g \lesssim 1.2$, with $\log g \simeq 0.8$ being typical.

Figures 8, 9, 10, 11, and 12 show the measured values of the G4300, Mg 1, Mg 2, Mg *b*, and Fe5406 indexes, respectively, plotted against $(V-I)_0$ for the confirmed And II members. Also shown are line indexes for Lick/IDS stan-

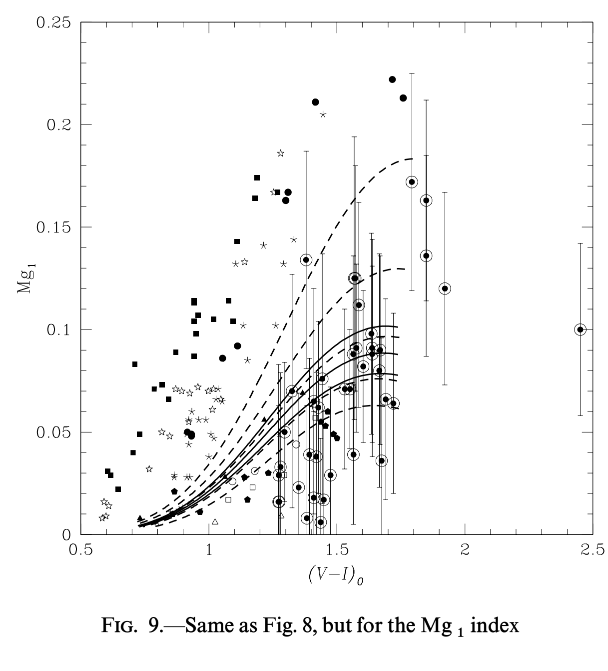

FIG. 9.—Same as Fig. 8, but for the Mg 1 index

TABLE 3

INDEX MEASUREMENTS FOR ANDROMEDA II MEMBERS

ID	G4300 (Å)	Mg 1 (mag)	Mg 2 (mag)	Mg *b* (Å)	Fe5406 (Å)	Comments
1	6.16 ± 0.50	0.033 ± 0.046	0.083 ± 0.047	1.23 ± 0.52	0.25 ± 0.05	
2	...	0.080 ± 0.057	0.276 ± 0.055	1.52 ± 0.33	2.46 ± 0.33	
4	5.37 ± 0.71	0.071 ± 0.039	0.153 ± 0.041	0.75 ± 0.36	2.49 ± 0.21	
5	5.79 ± 0.10	0.088 ± 0.043	0.164 ± 0.045	0.19 ± 0.10	2.59 ± 0.37	
6	6.26 ± 0.68	0.023 ± 0.046	0.066 ± 0.045	0.93 ± 0.38	1.11 ± 0.24	
7	...	0.112 ± 0.050	0.202 ± 0.051	1.43 ± 0.13	2.66 ± 0.07	
8	...	0.163 ± 0.049	0.249 ± 0.045	1.62 ± 0.18	3.24 ± 0.15	
10......	8.99 ± 2.65	0.062 ± 0.042	0.097 ± 0.046	0.21 ± 0.39	1.61 ± 0.04	
11......	7.97 ± 1.11	0.066 ± 0.039	0.100 ± 0.041	0.38 ± 0.67	1.41 ± 0.11	Mask 1
	7.15 ± 1.17	0.076 ± 0.043	0.118 ± 0.042	1.35 ± 0.05	2.35 ± 0.36	Mask 2
	7.65 ± 0.81	0.071 ± 0.029	0.109 ± 0.029	1.34 ± 0.05	1.49 ± 0.11	Average
12......	11.42 ± 0.61	0.120 ± 0.047	0.226 ± 0.051	0.19 ± 0.76	3.05 ± 0.05	
13......	6.38 ± 0.09	0.090 ± 0.046	0.216 ± 0.046	2.67 ± 0.67	3.49 ± 0.26	
14......	10.98 ± 2.51	0.100 ± 0.042	0.431 ± 0.049	5.74 ± 1.52	3.01 ± 0.07	
15......	7.24 ± 0.16	0.006 ± 0.041	0.063 ± 0.040	1.08 ± 0.12	0.40 ± 0.15	
16......	...	0.098 ± 0.049	0.176 ± 0.048	1.29 ± 0.85	2.41 ± 0.44	
17......	7.60 ± 0.85	0.038 ± 0.041	0.071 ± 0.039	0.16 ± 0.07	1.47 ± 0.20	
18......	5.10 ± 0.47	0.039 ± 0.034	0.082 ± 0.035	0.85 ± 0.73	0.91 ± 0.05	
19......	7.47 ± 1.01	0.050 ± 0.034	0.090 ± 0.033	0.58 ± 0.42	1.51 ± 0.09	
20......	4.31 ± 0.09	0.019 ± 0.044	0.050 ± 0.041	0.40 ± 0.58	0.43 ± 0.13	Mask 1
	4.46 ± 0.58	0.012 ± 0.046	0.087 ± 0.049	0.95 ± 0.68	...	Mask 2
	4.31 ± 0.09	0.016 ± 0.032	0.065 ± 0.031	0.63 ± 0.44	0.43 ± 0.13	Average
22......	2.64 ± 1.06	0.082 ± 0.037	0.145 ± 0.038	1.06 ± 1.10	2.03 ± 0.34	
23......	5.03 ± 0.32	0.016 ± 0.047	0.078 ± 0.047	1.11 ± 0.28	0.53 ± 0.05	
25......	...	0.076 ± 0.061	0.136 ± 0.063	2.19 ± 0.31	1.05 ± 0.08	
26......	...	0.125 ± 0.055	0.160 ± 0.052	0.62 ± 0.32	3.03 ± 0.11	
28......	...	0.125 ± 0.069	0.168 ± 0.067	2.31 ± 0.08	0.97 ± 0.40	
29......	...	0.065 ± 0.055	0.138 ± 0.057	0.89 ± 0.34	1.00 ± 0.06	
30......	...	0.088 ± 0.048	0.101 ± 0.047	...	1.98 ± 0.29	
32......	...	0.064 ± 0.044	0.206 ± 0.045	3.42 ± 0.05	2.20 ± 0.56	
33......	...	0.091 ± 0.053	0.176 ± 0.055	1.26 ± 0.67	3.16 ± 0.06	
34......	5.66 ± 2.38	0.039 ± 0.047	0.069 ± 0.049	0.52 ± 0.30	0.54 ± 0.18	
35......	...	0.134 ± 0.053	0.202 ± 0.052	1.32 ± 0.13	2.38 ± 0.63	
36......	...	0.066 ± 0.049	0.115 ± 0.049	...	2.39 ± 0.10	
37......	4.98 ± 0.28	0.029 ± 0.043	0.078 ± 0.043	0.22 ± 0.56	0.36 ± 0.83	
39......	...	0.172 ± 0.053	0.265 ± 0.057	2.65 ± 0.65	3.25 ± 0.07	
40......	...	0.036 ± 0.060	0.268 ± 0.060	1.26 ± 0.46	2.62 ± 0.63	
42......	6.81 ± 0.37	0.070 ± 0.057	0.107 ± 0.056	1.84 ± 0.55	1.11 ± 0.74	
43......	1.93 ± 0.09	0.008 ± 0.055	0.042 ± 0.059	...	2.13 ± 0.36	
44......	6.10 ± 0.09	0.091 ± 0.041	0.151 ± 0.041	1.19 ± 0.40	0.96 ± 0.50	
45......	5.78 ± 0.39	0.018 ± 0.042	0.061 ± 0.041	1.27 ± 0.63	1.42 ± 0.08	
47......	2.40 ± 1.21	0.029 ± 0.054	0.090 ± 0.053	...	0.32 ± 3.48	
48......	5.40 ± 0.08	0.017 ± 0.043	0.096 ± 0.044	1.38 ± 0.67	0.86 ± 0.04	
49......	2.90 ± 1.28	0.136 ± 0.049	0.232 ± 0.051	2.77 ± 0.35	0.63 ± 0.08	
50......	...	...	0.055 ± 0.063	2.43 ± 0.82	0.86 ± 0.18	

dard stars in a sample of nine globular and open clusters, which span a wide range in metallicity, supplemented by new measurements for the eight red giants in M13 listed in Table 2. For the standard stars, we have transformed the published $(V-K)_0$ colors to $(V-I)_0$ using equation (10) of von Braun et al. (1998). In each figure, we show the corresponding Lick/IDS fitting functions from Gorgas et al. (1993) and/or Worthey et al. (1994).[2] The dashed lines indicate the expected relations for $\log g = 0.8$ and five different choices of metallicity: Fe/H] $= -2.5$, -2.0, -1.5, -1.0 and -0.5 dex. As a demonstration of the gravity sensitivity of each index, the solid lines indicate the relations for the three cases of $\log\ g = 0.4$, 0.8 and 1.2, and $[\mathrm{Fe/H}] = -1.67 \pm 0.16$ dex. As explained below, this metallicity produces the best simultaneous match between the Lick/IDS fitting functions and the combined set of line indexes measured for the And II program stars.

For each line index, we have computed the χ^2 statistic for the appropriate Lick/IDS fitting function over the range -2.5 dex $\leq [\mathrm{Fe/H}] \leq 0.0$ dex in increments of $\Delta[\mathrm{Fe/H}] = 0.025$ dex. The value of [Fe/H] that produced the lowest χ^2 was then adopted as the best-fit mean metallicity. The small number (three to five) of very red stars

[2] These fitting functions are based primarily on the globular cluster abundance scale of Kraft (1979), whereas the metallicity scale of Harris (1996) was used to calibrate the *VI* giant branch technique employed in § 4.1. We note, however, that for the six globular clusters used in the calibration by Lick fitting functions, the two scales show a mean difference of only $\Delta[\mathrm{Fe/H}] = 0.03 \pm 0.10$ dex.

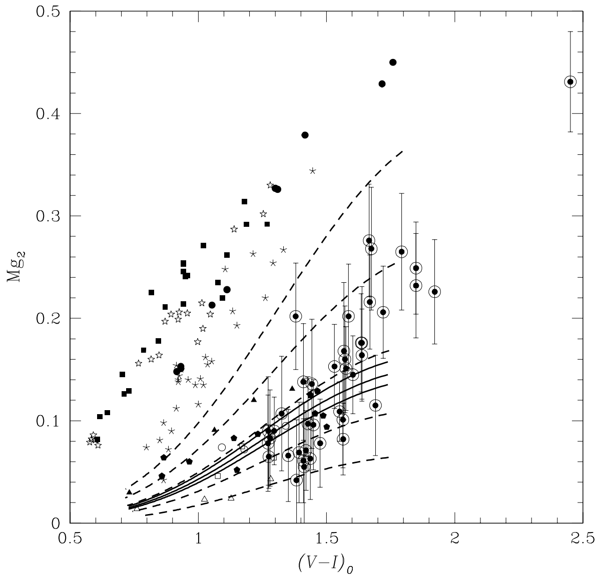

FIG. 10.—Same as Fig. 8, but for the Mg $_2$ index

having effective temperatures outside the range in which the fitting functions apply (as recommended by Gorgas et al. 1993 and Worthey et al. 1994) have been omitted from the χ^2 calculation. All measurements have been assigned equal weight. We have assumed log $g = 0.8$ for all And II program stars; the expected variations in surface gravity have a negligible effect on the derived metallicity (see, e.g., Figs. 8–12). For the five different indexes, we find best-fit mean metallicities of -1.42 (G4300), -2.16 (Mg_1), -1.54 (Mg_2), -1.90 (Mg b), and -1.33 (Fe5406) dex. The average of these five values is $\langle[Fe/H]\rangle = -1.67 \pm 0.16$ dex, where the quoted uncertainty refers to the error in the mean. This is our best estimate of the mean metallicity of the And II stars for which we have LRIS spectra. By comparison, if the measurements are weighted according to the inverse square

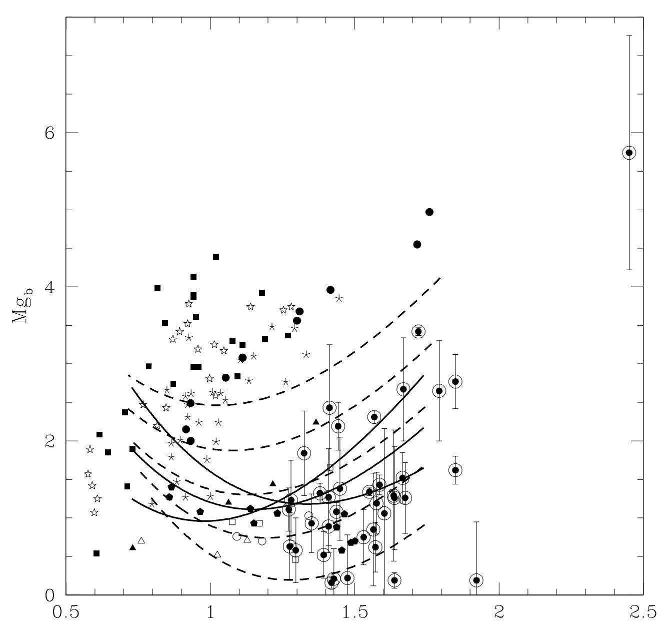

FIG. 11.—Same as Fig. 8, but for the Mg b index

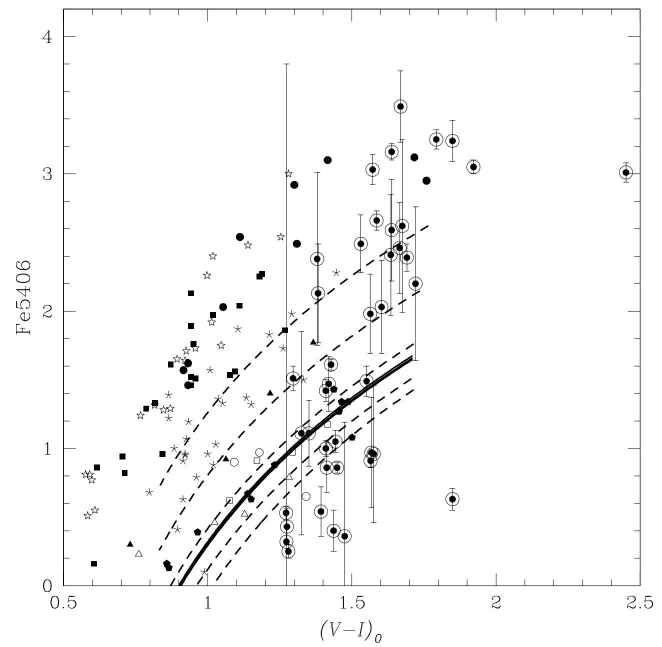

FIG. 12.—Same as Fig. 8, but for the Fe5406 index

of the index uncertainties, the respective metallicities are -1.67, -2.34, -1.62, -1.65 and -1.60 dex, with a mean of $\langle[Fe/H]\rangle = -1.78 \pm 0.14$ dex.

The above estimate of $\langle[Fe/H]\rangle = -1.67 \pm 0.16$ dex is biased since, as is evident in Figure 3, the most metal-poor giants are brighter than their metal-rich counterparts and will thus be preferentially included in our spectroscopic sample. The magnitude of this bias is easily calculated, however, by comparing the distribution in the (I, $V-I$)

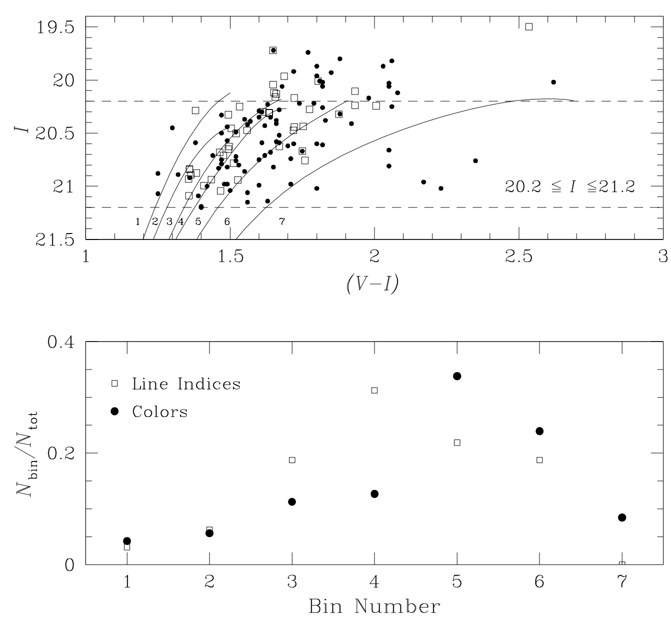

FIG. 13.—*Top*: Distribution in the color-magnitude plane of And II members having measured line indexes (*squares*) and $20.2 \leq I \leq 21.2$. Unresolved objects within this magnitude interval and located within 1′ of the galaxy's center are shown as circles. The globular cluster fiducial giant branches from Figs. 3 and 4 are indicated by the curves. *Bottom*: Fraction of stars in each metallicity bin (see text). Squares indicate the stars having measured line indexes; circles indicate the sample of objects having $V-I$ colors only.

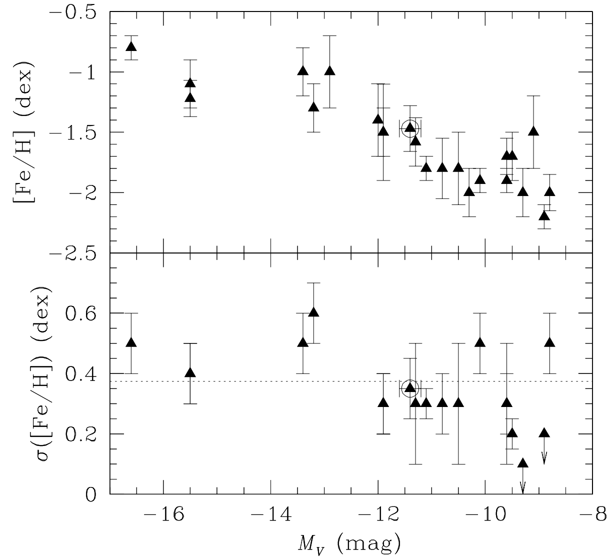

FIG. 14.—*Top*: Mean stellar metallicity plotted against absolute magnitude for Local Group dE, dSph, and dIrr/dSph galaxies. The data are from Mateo (1998), Armandroff et al. (1998, 1999), Grebel & Guhathakurta (1999), and Caldwell (1999). And II is indicated by the circled point. *Bottom*: Intrinsic dispersion in metallicity plotted against absolute magnitude for Local Group dE, dSph, and dIrr/dSph galaxies. The data are from Mateo (1998). The circled point indicates the location of And II. The dotted line indicates the mean dispersion of $\sigma([\mathrm{Fe/H}]) = 0.37 \pm 0.03$ dex (mean error).

CMD of the red giants with LRIS spectra to that of the entire sample of And II red giants. Figure 13 compares the distributions over the range $20.2 \leq I \leq 21.2$, i.e., the upper 1 mag of the RGB. For the photometric sample, we consider only those stars within 1′ of the galaxy's center in order to minimize contamination foreground stars and unresolved galaxies. The bottom panel of Figure 13 shows the relative number of stars located in seven "bins" defined by the globular cluster fiducial sequences shown in the top panel (i.e., bin 1 refers to the region blueward of the leftmost curve, bin 2 refers to the region between the two leftmost curves, etc.). Based on the distributions in the given in the bottom panel, we find that the mean metallicity of our spectroscopic sample is 0.2 ± 0.1 dex more metal-poor than the unbiased sample. Thus, our corrected estimate for the mean metallicity of And II is

$$\langle[\mathrm{Fe/H}]\rangle = -1.47 \pm 0.19 \text{ dex} .$$

This value is in close agreement with the value of $\langle[\mathrm{Fe/H}]\rangle = -1.59^{+0.44}_{-0.12}$ dex found by KNMF and is consistent with the somewhat higher value of $\langle[\mathrm{Fe/H}]\rangle = -1.35 \pm 0.3$ dex found in § 4.1 using the dereddened color of the galaxy's giant branch.

Can the spread in metallicity inferred from the wide giant branch evident in Figures 3 and 4 be confirmed spectroscopically? The uncertainties of the Mg *b* indexes are sufficiently small that it is possible to test this claim. Fitting a Gaussian to the residuals between the measured Mg *b* indexes and the best-fit relation shown in Figure 11 gives a dispersion of $\sigma(\mathrm{Mg}\ b) = 0.5 \pm 0.2$ Å. From Gorgas et al. (1993), we expect $d\,\mathrm{Mg}\ b/d\,[\mathrm{Fe/H}] \sim 1.7$ Å dex^{-1} over this range in color. Thus, the observed dispersion in Mg *b* corresponds to $\sigma([\mathrm{Fe/H}]) = 0.29 \pm 0.12$ dex, which, when combined with the findings of § 4.1, gives

$$\sigma([\mathrm{Fe/H}]) = 0.35 \pm 0.10 \text{ dex} ,$$

which we adopt as our best estimate for the intrinsic dispersion of And II.

5. COMPARISON WITH OTHER LOCAL GROUP DWARFS

In the top panel of Figure 14, we show the dependence of $\langle[\mathrm{Fe/H}]\rangle$ on galaxy magnitude for Local Group dE, dSph, and "dIrr-dSph transition" objects. The data are taken from Mateo (1998), supplemented by new observations from Armandroff et al. (1998, 1999), Grebel & Guhathakurta (1999), and Caldwell (1999). The measured metallicity of And II is consistent with that expected on the basis of its absolute magnitude and the well-known metallicity-luminosity relation for dwarf galaxies (Aaronson 1986; Caldwell et al. 1992). As the bottom panel of Figure 14 demonstrates, And II exhibits a spread in metallicity that is comparable in size to that found from spectroscopy of Galactic dSph's and photometry of several dSph companions of M31. The sample mean, $\sigma([\mathrm{Fe/H}]) = 0.37 \pm 0.03$ dex, is indicated by the dotted line.

Interestingly, available evidence seems to suggest that although the *mean* stellar metallicity in these galaxies—whose luminosities span a range of more than 3 orders of magnitude—depends rather sensitively on absolute magnitude, the *dispersion* in metallicity does not.[3] High-resolution spectroscopy of additional Galactic dSph's, such as that presented by Shetrone et al. (1998) for Draco, and intermediate-resolution spectroscopy for an expanded sample of M31 dwarf galaxies will help refine our understanding of the chemical enrichment histories of these galaxies.

The authors thank Christian König for sending us his Thuan-Gunn photometry and Ed Olszewski for providing coordinates of the four stars observed by Aaronson et al. (1985). P. C. acknowledges support provided by the Sherman M. Fairchild Foundation. The research of J. G. C. is supported, in part, by NSF grant 96-16729. The W. M. Keck Observatory is operated as a scientific partnership among the California Institute of Technology, the University of California, and the National Aeronautics and Space Administration. The observatory was made possible by the generous financial support of the W. M. Keck Foundation.

[3] The range in mass is a factor of ~ 20 if these dwarfs are embedded in dark halos of mass $M \sim 2 \times 10^7 M_\odot$, as proposed by Mateo et al. (1993) and Mateo (1998).

REFERENCES

Aaronson, M. 1983, ApJ, 266, L11
———. 1986, in Star Forming Dwarf Galaxies and Related Objects, ed. D. Kunth, T. X. Thuan, & J. Trân Thanh Van (Paris: Ed. Frontières), 125
Aaronson, M., Olszewski, E., Gordon, G. D., Mould, J. R., & Suntzeff, N. 1985, ApJ, 296, L7
Armandroff, T. E., Da Costa, G. S., Caldwell, N., & Seitzer, P. 1993, AJ, 106, 986
Armandroff, T. E., Davies, J. E., & Jacoby, G. H. 1998, AJ, 116, 2287
Armandroff, T. E., Jacoby, G. H., & Davies, J. E. 1999, AJ, in press
Bergbusch, P. A., & VandenBerg, D. A. 1992, ApJS, 81, 163
Caldwell, N. 1999, AJ, in press
Caldwell, N., Armandroff, T. E., Seitzer, P., & Da Costa, G. S. 1992, AJ, 103, 840
Canterna, R. 1975, ApJ, 200, 63
Cohen, J. G. 1979, ApJ, 231, 751
Cohen, J. G., Persson, S. E., & Frogel, J. A. 1978, ApJ, 222, 165
Côté, P., Hanes, D. A., McLaughlin, D. E., Bridges, T. J., Hesser, J. E., & Harris, G. L. H. 1997, ApJ, 476, L15
Côté, P., Mateo, M., Olszewski, E. O., & Cook, K. H. 1999, ApJ, in press
Da Costa, G. S. 1992, in IAU Symp. 149, The Stellar Populations of Galaxies, ed. B. Barbuy & A. Renzini (Dordrecht: Kluwer), 191
Da Costa, G. S., & Armandroff, T. E. 1990, AJ, 100, 162
Da Costa, G. S., Armandroff, T. E., Caldwell, N., & Seitzer, P. 1996, AJ, 112, 2576
Da Costa, G. S., Hatzidimitriou, D., Irwin, M. J., & McMahon, R. G. 1991, MNRAS, 249, 473
Dickens, R. J. 1972, MNRAS, 159, 7P
Faber, S. M., & Lin, D. N. C. 1983, ApJ, 266, L17
Fahlman, G. G., Richer, H. B., Searle, L., & Thompson, I. B. 1989, ApJ, 343, 49
Ferraro, F. R., Carretta, E., Corsi, C. E., Fusi Pecci, F., Cacciari, C., Buonanno, R., Paltrinieri, B., & Hamilton, D. 1997, A&A, 320, 757
Gebhardt, K., Pryor, C., Williams, T. B., & Hesser, J. E. 1994, AJ, 107, 2067
Gorgas, J., Faber, S. M., Burstein, D., Gonzalez, J. J., Courteau, S., & Prosser, C. 1993, ApJS, 86, 153
Grebel, E. K. 1999, in IAU Symp. 192, The Stellar Content of the Local Group, ed. P. Whitelock & R. Cannon (San Francisco: ASP), 1
Grebel, E. K., & Guhathakurta, P. 1999, ApJ, 511, L101
Harding, G. A. 1962, Observatory, 82, 205
Harris, W. E. 1996, AJ, 112, 1487
Holland, S. 1998, AJ, 115, 1916
Hopp, U., Schulte-Ladbeck, R. E., Greggio, L., & Mehlert, D. 1999, A&A, 342, 9
Ibata, R. A., Wyse, R. F. G., Gilmore, G., & Suntzeff, N. B. 1997, AJ, 113, 634
Karachentsev, I. D., & Karachentseva, V. E. 1999, A&A, 341, 355
Kells, W., Dressler, A., Sivaramakrishnan, A., Carr, D., Koch, E., Epps, H., Hilyard, D., & Pardeilhan, G. 1998, PASP, 110, 1487
König, C. H. B., Nemec, J. M., Mould, J. R., & Fahlman, G. G. 1993, AJ, 106, 1819 (KNMF)
Kraft, R. P. 1979, ARA&A, 17, 309
Landolt, A. U. 1992, AJ, 104, 340
Mateo, M. 1998, ARA&A, 36, 435
Mateo, M., Olszewski, E. W., Pryor, C., Welch, D. L., & Fischer, P. 1993, AJ, 105, 510
McClure, R. D. 1997, PASP, 109, 536
Monet, D., et al. 1996, USNO-A1.0 Catalog of Astrometric Standards (Washington: US Nav. Obs.)
Oke, J. B., et al. 1995, PASP, 107, 375
Schlegel, D. J., Finkbeiner, D. P., & Davis, M. 1998, ApJ, 500, 525
Shetrone, M. D., Bolte, M., & Stetson, P. B. 1998, AJ, 115, 1888
Smecker-Hane, T. A., Stetson, P. B., Hesser, J. E., & Lehnert, M. D. 1994, AJ, 108, 507
Stetson, P. B. 1987, PASP, 99, 191
———. 1993, in IAU Colloq. 136, Stellar Photometry: Current Techniques and Future Developments, ed. C. J. Butler & I. Elliot (Cambridge: Cambridge Univ. Press), 291
Stetson, P. B., Hesser, J. E., & Smecker-Hane, T. A. 1998, PASP, 110, 533
Suntzeff, N. B., Mateo, M., Terdrup, D. M., Olszewski, E. W., Geisler, D., & Weller, W. 1993, ApJ, 418, 208
Taylor, B. J. 1986, ApJS, 60, 577
van den Bergh, S. 1972, ApJ, 171, L31
von Braun, K., Chiboucas, K., Minske, J. K., Salgado, J. F., & Worthey, G. 1998, PASP, 110, 810
Worthey, G., Faber, S. M., Gonzalez, J. J., & Burstein, D. 1994, ApJS, 94, 687
Zinn, R. 1978, ApJ, 225, 790